II CONGRESSO NACIONAL DE ENGENHARIA MECÂNICA
II NATIONAL CONGRESS OF MECHANICAL ENGINEERING
12 a 16 de Agosto de 2002 - João Pessoa – PB

ANALYZING VIBROIMPACTS OF SLENDER BEAMS THROUGH KARHUNEN-LOÈVE EXPANSION

Claudio Wolter
Laboratório de Dinâmica e Vibrações, Pontifícia Universidade Católica do Rio de Janeiro, 22453-900
cwolter@mec.puc-rio.br
Marcelo A. Trindade
Laboratório de Dinâmica e Vibrações, Pontifícia Universidade Católica do Rio de Janeiro, 22453-900
trindade@mec.puc-rio.br
Rubens Sampaio
Laboratório de Dinâmica e Vibrações, Pontifícia Universidade Católica do Rio de Janeiro, 22453-900
rsampaio@mec.puc-rio.br

Abstract. *This work presents a study of the oscillations of a non-rotating drillstring, represented here by a vertical slender beam, clamped in its upper extreme, pinned in its lower one and constrained inside an outer cylinder in its lower portion. The beam is subjected to distributed axial loads, due to its own weight, leading to geometric softening of its lower portion and thus yielding a large number of vibroimpacts with the outer cylinder. This is due to the axial-bending coupling, often called geometric stiffening and largely discussed in the last two decades. Here, it is accounted for by using a non-linear finite element model proposed in a previous work, in which non-linear strain-displacement relations are considered. To help understand this nonlinear coupled vibroimpact problem, the Karhunen-Loève decomposition, also known as the proper orthogonal decomposition, is applied to its simulated dynamics. The results show that the micro-impacts, accompanying the bottom-hole impacts and mainly due to the beam compressive softening, and the reaction forces at the bottom position, are well represented only when using a non-linear axial/bending coupling. It is also shown that 15 proper orthogonal modes are sufficient to reconstruct the dynamics of the impacting beam under a 3% error margin.*

Keywords: *Karhunen-Loève Expansion, Vibroimpact, Axial-Bending Coupling, Finite Element*

1. INTRODUCTION

It is well-known that flexible beams subjected to axial loads present strong stiffness variations. This is due to what is often called *geometric stiffening effect* in the literature (Sharf, 1995). It may also be seen as a consequence of the coupling between axial and bending strains. In the last two decades, several methodologies have been proposed to account for the geometric stiffening effect. In particular, Simo and Vu-Quoc (1987) showed that modeling beams under large rotations using linear beam theories results in a spurious loss of stiffness and hence they proposed a “consistent” linearization using steady-state values for the axial internal force. Kane *et al.* (1987) proposed a methodology, that uses higher order strain measures, and applied it to the dynamics of a cantilever beam under prescribed large translation and rotation. Some of these models were summarized and compared by Trindade and Sampaio (2002) using a general non-linear model, resulting from non-linear strain-displacement relations. Their conclusion is that a non-linear model with coupled axial/bending vibrations is required for an accurate representation of the dynamics of slender beams.

Due to the non-linearity induced by the geometric stiffening, augmented by the intrinsic non-linear behavior of dynamics of structures subjected to impacts, one is obliged to consider non-linear analysis techniques. The Karhunen-Loève (KL) decomposition, also known as the proper orthogonal decomposition, is a powerful tool for obtaining spatial information and providing a basis for model reduction of non-linear structural systems (Sirovich, 1987). It consists in obtaining a set of orthogonal eigenfunctions (or proper orthogonal modes) where the dynamics is to be projected. This set of KL modes are optimal in the sense that it minimizes the error of the approximation for any number of modes considered, meaning that no other linear expansion may lead to a better representation of the response with the same number of modes. Indeed, Steindl and Troger (2001) concluded that KL modes are by far the best choice for a standard Galerkin approximation. Practically, the KL decomposition is obtained by constructing a spatial autocorrelation tensor from the simulated or measured dynamics of the system. Thereafter, performing its spectral decomposition, one finds that the spatial autocorrelation tensor eigenfunctions provide the required proper orthogonal modes and its eigenvalues represent the mean energy contained in that projection. This technique was previously used for the analysis of vibroimpact problems by Azeez and Vakakis (2001) and Wolter and Sampaio (2001).

Here, the vibrations of a non-rotating drillstring, represented here by a vertical slender beam, clamped in its upper extreme, pinned in its lower one and constrained inside an outer cylinder in its lower portion, are studied. The beam is subjected to distributed axial loads, due to its own weight, leading to geometric softening of its lower portion and, thus, to vibroimpacts with the outer cylinder. To help understand this nonlinear vibroimpact problem, the KL decomposition is applied to its simulated dynamics, which is evaluated using an extension of the non-linear finite element (FE) model proposed in a previous work (Trindade and Sampaio, 2002).

2. NON-LINEAR MODEL FORMULATION

Let us consider an initially straight and slender cylinder, of undeformed length L and outer and inner radii R_o and R_i, undergoing large displacements and small deformations.

2.1. Theoretical Formulation

Small deformations are assumed so that the beam cross-section rotation angle β is small. Also, the assumption of negligible shear strains, leading to $\beta = -v'$, is considered. Notice that the prime denotes the derivative with respect to the axial coordinate x. Consequently, the displacement vector $\mathbf{p}$ of a given point with position $\mathbf{X}$ in the xz plane is

$$\mathbf{p} = \begin{Bmatrix} u - zv' \\ v \end{Bmatrix} \quad , \quad \text{for } \mathbf{X} = \begin{Bmatrix} x \\ z \end{Bmatrix} \tag{1}$$

where x and z directions are such that $0 \leq x \leq L$ and $-R_o \leq z \leq R_o$. Here, only the axial component of the Lagrangian strain tensor $\varepsilon_{xx} \equiv E_{11}$ is considered. Therefore, defining the axial displacement as $u_0 = u - zv'$, the non-linear axial strain ε_{xx} may be written in the following form

$$\varepsilon_{xx} = u_0' + \frac{1}{2}\left[(u_0')^2 + (v')^2\right] \tag{2}$$

From the assumption of negligible shear strains and also neglecting the contribution of transverse normal stress σ_{zz}, the strain potential energy of the beam is

$$H = \frac{1}{2}\int E\varepsilon_{xx}^2 \, \mathrm{d}V = \frac{1}{2}\int_0^L \left[EA\left(u'^2 + \underline{u'v'^2 + 1/4v'^4} + \underline{\underline{u'^3 + 1/4u'^4}} + \underline{\underline{1/2u'^2v'^2}} \right) \right.$$
$$\left. + EI\left(v''^2 + \underline{\underline{3u'v''^2 + 3/2u'^2v''^2 + 3h^2/20v''^4}} + \underline{\underline{1/2v'^2v''^2}} \right) \right] \, \mathrm{d}x \tag{3}$$

where E is the Young's modulus of the beam and by considering a symmetric beam cross-section with respect to z-axis and using (2), the potential energy of the beam was written in terms of the mean axial u and transversal v displacements only. A and I are the area and moment of inertia of the beam cross-section. Single underlined terms in (3) are due to the presence of term $(v')^2$, quadratic in the cross-section rotation angle $\beta = -v'$, in the axial strain ε_{xx}. Notice that they appear only in the membrane strain component, unlike double and triple underlined terms that are present in both membrane and bending components of the strain energy. The term $(u_0')^2$, quadratic in the axial displacement derivative, of the axial strain (2) leads to the double underlined terms in the strain energy function, while triple underlined terms are due to the coupling between the two quadratic terms of the axial strain. It is worthwhile to notice also that the assumption of linear strain-displacement relation eliminates all underlined terms of (3).

In the present work, only the contributions of cubic and lower order terms in u_0' and v' are retained in the potential energy (3). From the definition of u_0, this leads to a potential energy,

$$H_s = \frac{1}{2}\int_0^L \left[EA\left(u'^2 + \underline{u'v'^2} + \underline{\underline{u'^3}}\right) + EI\left(v''^2 + \underline{\underline{3u'v''^2}}\right)\right]\,\mathrm{d}x \tag{4}$$

The kinetic energy of the beam may also be written in terms of the main variables u and v. Hence, starting from the general form of the kinetic energy in terms of the total displacement of the beam and then using (1) and assuming symmetric beam cross-section with respect to z-axis, the kinetic energy of the beam, in terms of the main variables u and v, is

$$T = \frac{1}{2}\int \rho\dot{\mathbf{p}}^T\dot{\mathbf{p}}\,\mathrm{d}V = \frac{1}{2}\int_0^L \left[\rho A\left(\dot{u}^2 + \dot{v}^2\right) + \rho I\dot{v}'^2\right]\,\mathrm{d}x \tag{5}$$

where ρ is the beam mass density and $\dot{\mathbf{p}}$ is the velocity vector. The terms in (5) correspond to inertia contributions due to translation, in x and z directions, and cross-section rotation.

The beam is subjected to its own weight, which may be expressed as vertical forces (in x-direction) due to the gravity field. Assuming symmetric cross-section, their work may be written as

$$W = \int \mathbf{p}^T\mathbf{f}_g\,\mathrm{d}V = \int_0^L \rho g A u\,\mathrm{d}x \quad ; \quad \text{with } \mathbf{f}_g = \begin{Bmatrix}\rho g\\ 0\end{Bmatrix} \tag{6}$$

Using the expressions for strain (4) and kinetic (5) energies and work due to gravity forces (6) presented above, a variational formulation is used in this section to derive the FE model.

The virtual variation of the simplified strain energy H_s is decomposed in linear and non-linear contributions arising from the non-linear strain-displacement relations (2) and, hence, is written as

$$\delta H_s = \delta H_{sl} + \delta H_{sn} \tag{7}$$

where the linear δH_{sl} and non-linear δH_{sn} contributions are expressed in terms of the variations $\delta u'$, $\delta v'$ and $\delta v''$ as follows

$$\delta H_{sl} = \int_0^L \left(\delta u' EAu' + \delta v'' EIv''\right)\,\mathrm{d}x \tag{8}$$

$$\delta H_{sn} = \int_0^L \left[\frac{1}{2}\delta u' EA\left(3u'^2 + v'^2\right) + \frac{3}{2}\delta u' EIv''^2 + 3\delta v'' EIu'v'' + \delta v' EAu'v'\right]\,\mathrm{d}x \tag{9}$$

Notice that the non-linear contributions δH_{sn} come from the underlined terms in (4). On the other hand, the linear contributions δH_{sl} are the standard ones for Euler-Bernoulli beams.

The virtual variation of the kinetic energy T may be derived from (5), which through integration in time is equivalent to

$$\int_{t_1}^{t_2}\delta T = -\int_{t_1}^{t_2}\int_0^L \left[\rho A\left(\delta u\ddot{u} + \delta v\ddot{v}\right) + \rho I\delta v'\ddot{v}'\right]\,\mathrm{d}x \tag{10}$$

This expression may also be interpreted as the virtual work done by the inertial forces, composed of translation in x and z directions and cross-section rotation in the xz plane.

The virtual work done by the gravity forces is obtained from (6) and is written in terms of δu only since these forces keep their vertical x direction under deformation.

$$\delta W = \int_0^L \rho g A \delta u \, \mathrm{d}x \tag{11}$$

2.2. Non-linear Finite Element Model

The FE model is constructed through discretization of the virtual variations of strain (7) and kinetic (10) energies. Although some terms in the strain energy (3) were still neglected, it is assumed for now that the main contributions to the axial-bending coupling should be accounted for by the terms considered in (4). The discretization is carried out using Lagrange linear shape functions for the axial displacement u and Hermite cubic ones for the transversal deflection v. This leads to six degrees of freedom $\mathbf{q}^T = \{u_1 \; v_1 \; \beta_1 \; u_2 \; v_2 \; \beta_2\}$, where $(\beta_1, \beta_2) = (v_1', v_2')$. Moreover, the axial and transversal displacements are discretized as follows

$$u = \mathbf{N}_u \mathbf{q} \quad ; \quad v = \mathbf{N}_v \mathbf{q} \tag{12}$$

where, the operators $\mathbf{N}_u$ and $\mathbf{N}_v$ are written in terms of the adimensional axial position $\xi = x/L$, as $\mathbf{N}_u = [1-\xi \; 0 \; 0 \; \xi \; 0 \; 0]$ and $\mathbf{N}_v = [0 \; 1-3\xi^2+2\xi^3 \; \xi L(1-\xi)^2 \; 0 \; \xi^2(3-2\xi) \; \xi^2 L(\xi-1)]$. Replacing the discrete expressions for the displacements and their derivatives in the linear and non-linear contributions to the virtual variation of strain energy, (8) and (9), leads to

$$\delta H_{sl} = \delta \mathbf{q}^T \mathbf{K}_e \mathbf{q} \; ; \; \delta H_{sn} = \delta \mathbf{q}^T \mathbf{K}_g \mathbf{q} \tag{13}$$

where these define the linear elastic stiffness $\mathbf{K}_e$ and non-linear geometric stiffness $\mathbf{K}_g$ matrices.

The discretization of the virtual work of inertial (10) and gravity (11) forces, yields

$$\int_{t_1}^{t_2} \delta T \, \mathrm{d}t = -\int_{t_1}^{t_2} \delta \mathbf{q}^T \mathbf{M} \ddot{\mathbf{q}} \, \mathrm{d}t \quad \text{and} \quad \delta W = \delta \mathbf{q}^T \mathbf{F}_g \tag{14}$$

Therefore, the discretized virtual variations may be introduced in Hamilton's principle, which, from (13) and (14) and after assembling all elements, yields the following equations of motion

$$\mathbf{M}\ddot{\mathbf{q}} + [\mathbf{K}_e + \mathbf{K}_g(\mathbf{q})]\mathbf{q} = \mathbf{F}_g \tag{15}$$

where $\ddot{\mathbf{q}}$ defines the acceleration vector. Point forces and damping matrices may be imposed a posteriori to the system. The symmetric linear elastic stiffness matrix $\mathbf{K}_e$ corresponds to the standard Euler-Bernoulli beam with axial and bending stiffnesses. $\mathbf{K}_g$ states for the geometric stiffness which, as presented previously, depends on the configuration and thus corresponds to the non-linear terms in the equations of motion. These mass and stiffness matrices are not presented here due to lack of space. However, as shown by Trindade and Sampaio (2002), the bending stiffness varies linearly with the relative axial displacement $\tilde{u} = u_2 - u_1$. That is, this stiffness increases when $\tilde{u}$ is positive and decreases in the opposite case. This is in agreement with the notion that the beam is stiffer when under extension and, on the contrary, it is less stiff when under axial compression.

2.3. Accounting for Initial Deformed Configuration

In this section, the non-linear FE model is applied to a vertical slender beam clamped at its top position, axially sliding at its bottom position and subjected to its own weight. Hence, the boundary conditions considered here are: all degrees of freedom locked at the top position and transversal displacement locked at the bottom position. Figure 1 presents the idealized undeformed and deformed

configurations for the vertical slender beam. In addition to gravity forces, a negative axial force is applied at the bottom position to simulate the static reaction force when the beam touches the bottom. Therefore, the equations of motion (15) may be rewritten as

$$\mathbf{M}\ddot{\mathbf{q}} + [\mathbf{K}_e + \mathbf{K}_g(\mathbf{q})]\mathbf{q} = \mathbf{F}_g - \mathbf{F}_f \tag{16}$$

In the practical case, the beam is lowered until its free end touches the bottom position, which is inside the hole. In the event of continued lowering of the beam, the reaction force $\mathbf{F}_f$, applied to the beam free end, grows and the lower part of the beam is compressed. In the present work, it is supposed that after this quasi-static lowering and when the reaction force reaches a given value, the axial displacement of the beam tip is locked (Figure 1b). Therefore, further motions occur around this deformed configuration, which is the solution of the following equation,

$$\mathbf{q}_s = \mathbf{K}_e^{-1}(\mathbf{F}_g - \mathbf{F}_f) \tag{17}$$

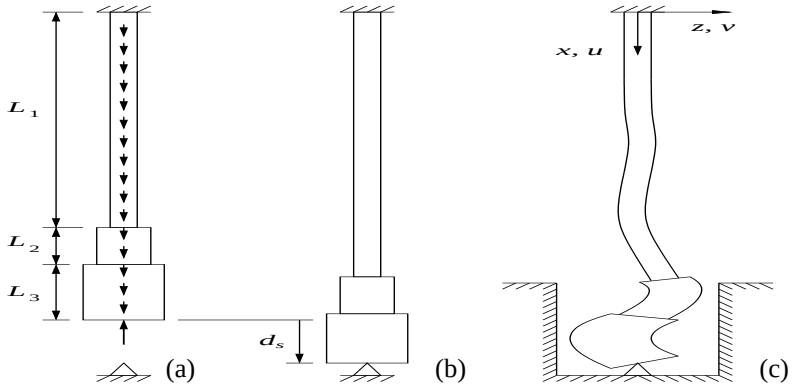

Figure 1: Undeformed and deformed configurations for the vertical slender beam.

Let us define then a new displacement vector $\bar{\mathbf{q}}$ relative to the static one $\mathbf{q}_s$, as $\bar{\mathbf{q}} = \mathbf{q} - \mathbf{q}_s$. Substituting $\mathbf{q}$ by $\bar{\mathbf{q}} + \mathbf{q}_s$ in (16) and accounting for (17), one may write a new set of equations of motion in terms of the relative displacements vector $\bar{\mathbf{q}}$. The axial displacement of the beam bottom tip is then locked into its static value, such that $\bar{u}^L = 0$, or $u^L = u_s^L$. The equations of motion then become,

$$\mathbf{M}_r\ddot{\bar{\mathbf{q}}}_r + [\mathbf{K}_{er} + \mathbf{K}_{gr}(\bar{\mathbf{q}} + \mathbf{q}_s)]\bar{\mathbf{q}}_r = \mathbf{0} \tag{18}$$

Notice that the reduced mass and stiffness matrices are those for axial and transversal displacements locked at the bottom position (that is, a clamped-hinged beam, as shown in Figure 1c). The global response is then obtained through summation of the relative displacements, augmented by the nil relative axial displacement at bottom position $\{\bar{\mathbf{q}}_r^T \ 0\}^T$, with the static displacements $\mathbf{q}_s$.

To account for bottom-hole impacts, an additional point force vector $\mathbf{F}_c$ is included in the model. Since it is supposed that the impacts occur only after lowering and locking the beam, the impact forces vector may be included directly in the equations of motion (18). Hence, the vector $\mathbf{F}_c$ is composed of nodal impact forces f_c^j that depend on whether the corresponding node j is in contact with the borehole, and respects the following law

$$f_c^j(t) = \begin{cases} 0, & \text{if } |v^j(t)| \le \varepsilon, \\ -k\{|v^j(t)| - \varepsilon \ \text{sign}[v^j(t)]\}, & \text{if } |v^j(t)| > \varepsilon, \end{cases} \tag{19}$$

where ε is the distance between the outer surface of the beam and the borehole wall and v^j is the transversal displacement of the node j. One may notice from (19) that the impact force is supposed to be linear elastic, with spring constant k, when there exists bottom-hole contact and zero otherwise. It is also supposed to be composed of a transversal component only, that is, friction effect is neglected. Hence, the equations of motion (18) are rewritten to account for the bottom-hole impact forces as

$$\mathbf{M}_r\ddot{\bar{\mathbf{q}}}_r + [\mathbf{K}_{er} + \mathbf{K}_{gr}(\bar{\mathbf{q}} + \mathbf{q}_s)]\bar{\mathbf{q}}_r = \mathbf{F}_c \tag{20}$$

3. NUMERICAL RESULTS

In the two following sections, the dynamics of a slender beam of special interest is simulated with MATLAB ode15s algorithm, using the non-linear FE model presented previously, and analyzed with the help of the KL decomposition. The strategy shown in the previous section to account for the initial deformation state is also used. A slender steel cylinder, representing a typical configuration of a drillstring used for oilwell drilling (Sotomayor, Plácido and Cunha, 1997), is considered here. Its geometrical properties are: $R_{o1} = 0.064$ m, $R_{i1} = 0.054$ m, $L_1 = 1700$ m; $R_{o2} = 0.064$ m, $R_{i2} = 0.038$ m, $L_2 = 100$ m; and $R_{o3} = 0.102$ m, $R_{i3} = 0.038$ m, $L_3 = 200$ m. The cylinder is divided in three different cross-sections. The upper portion, composed of drill pipes, is normally subjected to large traction forces and hence is much less flexible in bending than the rest of the drillstring, consequently possessing small outer diameter and thin wall. On the other hand, the lower portion, denoted as drill collars, is highly compressed by the weight of the upper part and thus is subjected to higher bending effects. That is why its outer diameter is much larger and its wall much ticker. As for the transition portion, denoted as heavy weight drill pipes, located between the drill pipes and the drill collars, it has the outer diameter of the drill pipes and the inner diameter of the drill collars.

The lower portion of the drillstring is confined inside a borehole of radius $R_h = 0.156$ m and has two stabilizers located 25 and 50 meters away from the drill bit. In this work, the stabilizers are accounted for by locking the beam transversal displacements at their positions. The spring constant considered for the elastic impact forces is $k = 10^8$ N/m and the clearance ε is obtained from the difference between the radii of the borehole and drillstring sections, $\varepsilon = R_h - R_o$. As explained in the previous section, the axial displacement of the drill bit is locked into its static deformed position. A static axial reaction force at the bottom position of $f = 200$ KN is considered. In addition, a sinusoidal perturbation moment, $50 \sin 2\pi t$ KN.m, is applied to the hinged bottom position to simulate bit-formation induced lateral vibration. The axial displacements, which are supposed to be initially at their static values, can be excited only through coupling with bending vibrations.

3.1. Drillstring Dynamics Simulation

The evolution of axial displacement at a position 6.25 m from the drill bit is shown in Figure 2, for both linear and non-linear models. One may observe that the axial displacement is very small for the linear model. This is due to the fact that, in this model, axial displacement is not coupled to the transversal displacement, which is the only one excited by the perturbation force considered. Indeed, these values for the axial displacement are believed to be due to numerical integration errors. On the other hand, it is clear from the results for the non-linear model (Figure 2b) that the axial displacement is not that small. Although much smaller than the static axial displacement, which is the reason why it is generally neglected, the effect of its variation relative to the static one will be evidenced later.

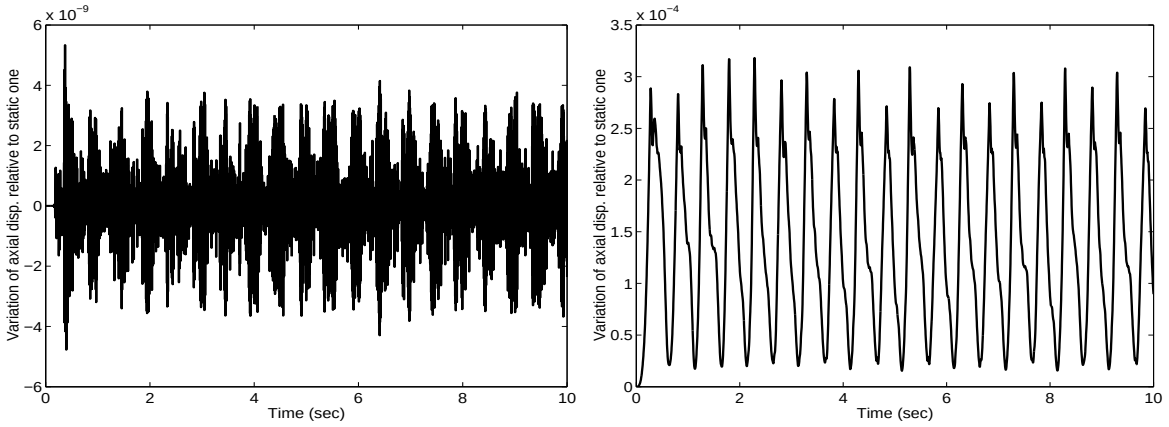

(a) (b)

Figure 2: Axial displacement at 6.25 m from the drill bit using linear (a) and non-linear (b) models.

Figure 3 shows the transversal displacement on the bottom portion of the drill collar, evaluated through integration in time of the linear (Figure 3a) and non-linear (Figure 3b) equations of motion. The bottom portion-hole clearance is also shown in the figure, by which one may notice that the drill collar is continuously under impact with the hole wall. This is in part due to the excitation at the drill bit and in part due to the bending flexibility caused by the compression of the lower portion of the drillstring. To improve clarity, the first impact instant is also shown in detail for linear and non-linear models. A comparison between Figures 3a and 3b shows that the non-linear model leads to a larger number of micro-impacts than the linear one. This is probably due to the higher flexibility of the beam, caused by the axial-bending coupling, only accounted for in the non-linear model.

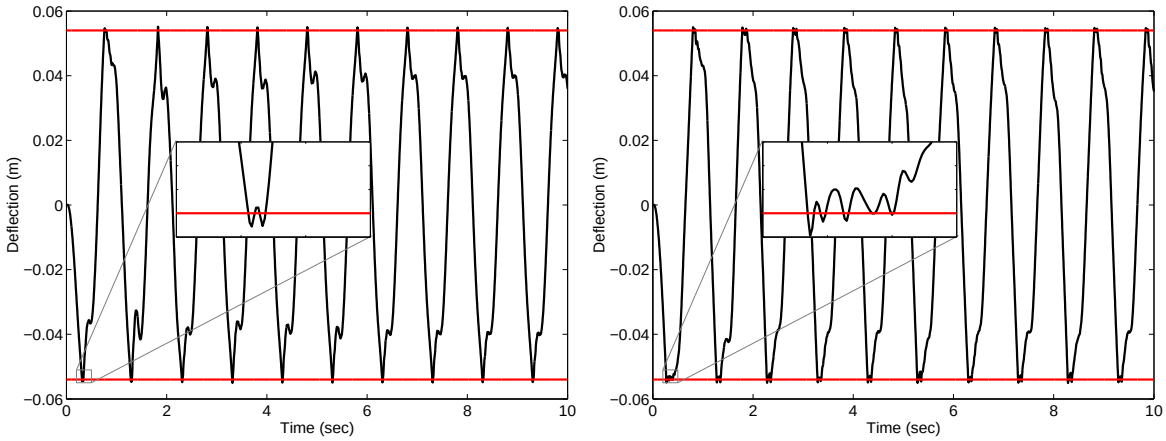

(a) (b)

Figure 3: Deflection at 6.25 m from the drill bit using linear (a) and non-linear (b) models.

The effect of non-linear coupling between axial and transversal vibrations is specially evidenced in the following analysis of the reaction forces. Figure 4 shows the reaction forces at the bottom position using linear (Figure 4a) and non-linear (Figure 4b) models. From Figure 4a, one concludes that the reaction force at the bottom position may be positive. This means that the drill bit is pulled from the bottom position, making it possible for the drill bit to loose contact with the formation for the larger values of deflection. This is clearly prevented here, since the axial displacement of the drill bit is locked into its static value. Nevertheless, the decrease in the force magnitude leads to a worse drilling performance. On the other hand, analysis of Figure 4b shows an increase in the force magnitude due to lateral vibration. This may be explained by the fact that the transversal displacement induces an increase in the axial displacement, leading to an augmentation of the compression in the bottom portion of the drill collar, instead of inducing its traction. This effect of compression or traction may vary according to the drillstring parameters and to the static value of the reaction force.

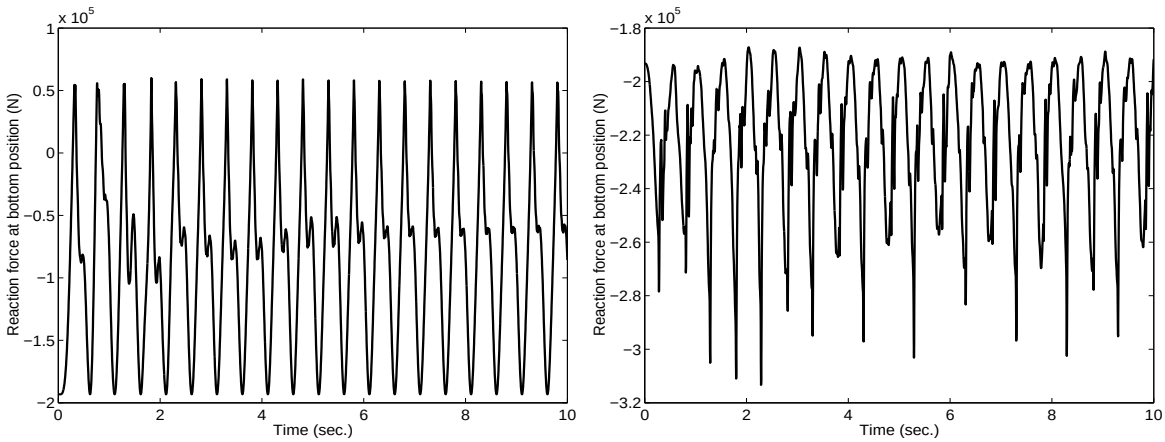

(a) (b)

Figure 4: Reaction forces at the bottom position using linear (a) and non-linear (b) models.

3.2. Karhunen-Loève Decomposition of the Response

In this section, the direct method of Karhunen-Loève decomposition (Wolter and Sampaio, 2001) is applied to the drillstring dynamics. For this purpose, the time response $\mathbf{q}(t)$ is subtracted from its mean $E[\mathbf{q}(t)]$ to obtain the deviation $\mathbf{q}_d(t) = \mathbf{q}(t) - E[\mathbf{q}(t)]$ of the time response. Consequently, the new vector $\mathbf{q}_d(t)$ has elements with zero mean. As the time response $\mathbf{q}(t)$, and thus also $\mathbf{q}_d(t)$, results from time integration of the discretized equations of motion (20), it is in fact sampled in M instants of time $t_1, t_2, \ldots, t_M$, chosen in the time integration algorithm. Hence, the time response $\mathbf{q}(t)$ may be written as a sampling matrix of dimension $M \times N$,

$$\mathbf{q} = \begin{bmatrix} q_1(t_1) & q_2(t_1) & \ldots & q_N(t_1) \\ q_1(t_2) & q_2(t_2) & \ldots & q_N(t_2) \\ \vdots & \vdots & \ddots & \vdots \\ q_1(t_M) & q_2(t_M) & \ldots & q_N(t_M) \end{bmatrix} \tag{21}$$

where each column represents the time response of a given degree of freedom from the FE mesh, with N being the total number of degrees of freedom or the dimension of $\mathbf{q}(t)$. Alternatively, each row represents the spatial distribution of the response at a given time instant, that is, a point in the N-dimensional phase space.

Using the ergodicity assumption, the mean value $E[\mathbf{q}(t)]$ may be obtained by the time average of $\mathbf{q}$, that is $\sum_i^M \mathbf{q}(t_i)/M$. Hence, the deviation $\mathbf{q}_d(t)$ with respect to the mean may also be written as a sampling matrix, obtained by subtracting from each line of $\mathbf{q}$ the time average of all rows,

$$\mathbf{q}_d = \mathbf{q} - \mathbf{q}_E \; ; \;\; \text{where } \mathbf{q}_E = \frac{1}{M} \begin{bmatrix} \sum_{i=1}^M q_1(t_i) & \sum_{i=1}^M q_2(t_i) & \ldots & \sum_{i=1}^M q_N(t_i) \\ \vdots & \vdots & \ddots & \vdots \\ \sum_{i=1}^M q_1(t_i) & \sum_{i=1}^M q_2(t_i) & \ldots & \sum_{i=1}^M q_N(t_i) \end{bmatrix} \tag{22}$$

The spatial autocorrelation matrix is then written in terms of the zero-mean time response sampling matrix as

$$\mathcal{R} = \frac{1}{M} \mathbf{q}_d^T \mathbf{q}_d \tag{23}$$

where $\mathcal{R}$ is, by definition, symmetric and positive semi-definite. Hence, its eigenvectors form an orthogonal basis and its eigenvalues are non-negative. In this case, the eigenvectors Ψ_j are the coherent structures or proper orthogonal modes (POMs) and the corresponding eigenvalues λ_j, or proper orthogonal values (POVs), give a measure of the mean energy contained in each mode, defined as

$$\mathcal{R}\Psi = \Lambda\Psi \; ; \text{ with } \Psi = [\Psi_1 \; \Psi_2 \; \cdots \; \Psi_N] \;\; \text{and} \;\; \Lambda = \text{diag}(\lambda_1, \lambda_2, \ldots, \lambda_N) \tag{24}$$

Notice that the autocorrelation matrix $\mathcal{R}$ has dimension $N \times N$. Hence, its dimension, and so the number of proper orthogonal modes and values, depend only on the number of degrees of freedom and not on the time instants used for the sampling of the time response.

The time response sampling matrix $\mathbf{q}$ may then be reconstructed, in a truncated basis, by expressing $\mathbf{q}$ in terms of its time average matrix $\mathbf{q}_E$ and a reduced number K of evaluated POMs as

$$\mathbf{q} = \sum_{j=1}^{K} A_j \Psi_j^T + \mathbf{q}_E \tag{25}$$

where the vectors of time coefficients A_j are easily found by projecting the time response onto each POM Ψ_j, that is, $A_j = \mathbf{q}\Psi_j$. Notice that, by definition, the POVs also respect the following relation with the time coefficients

$$\lambda_j = \frac{1}{M} \sum_{i=1}^{M} A_j^T A_j \tag{26}$$

Next, this procedure is applied to the drillstring dynamics response resulting from the integration of the equations of motion (20). Moreover, one expects to obtain additional information through analysis of the POMs and POVs. These are also used to construct an optimal basis, with minimum dimension, that allows us to project the equations of motion and obtain a reduced order model, well representing the main features of the response.

Figure 5 shows the first five POMs evaluated from the drillstring dynamics response $\mathbf{q}$, zoomed in its bottom portion, and the corresponding proper orthogonal values λ_j. It is worthwhile noting that the POVs where normalized so their sum is unitary. One may observe that most of the energy (89%) is contained in the first two POMs and that only the bottom portion of the drillstring presents transversal deflections. This is clearly due to the fact that the upper portion of the drillstring is under traction and thus is much stiffer in bending than the bottom portion that is under compression.

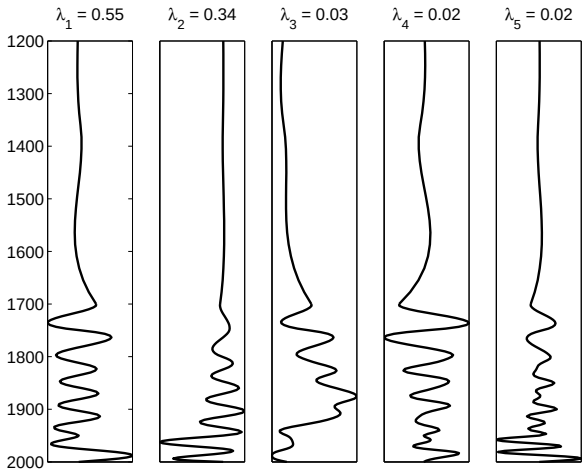

Figure 5: First five proper orthogonal modes evaluated from the transversal displacement response.

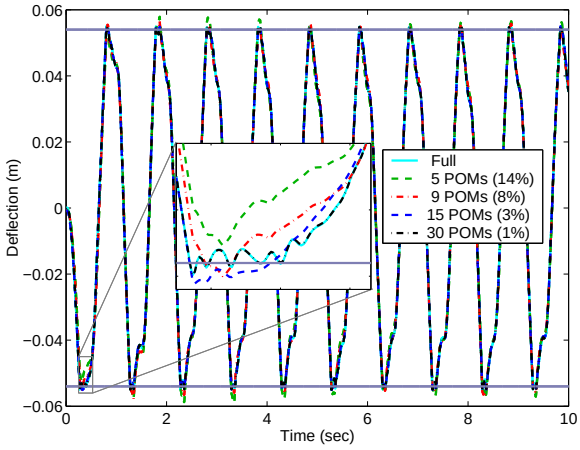

Figure 6: Reconstruction of the transversal displacement response using the first five, nine, fifteen and thirty proper orthogonal modes.

The first five POMs are responsible for 97% of the response. However, it is generally recommended to consider a number of modes sufficient to sum 99.9% of the response energy (Sirovich, 1987). Figure 6 shows the reconstruction of the transversal displacement response using the first 5, 9, 15 and 30 POMs. The percentage of the energy contained in these first POMs are respectively, 96.6567%, 99.1286%, 99.8613% and 99.9918%. Thus, 15 modes are needed to reconstruct the response, which is a great reduction of the model dimension, since the FE model contains 87 degrees of freedom. Nevertheless, one could also use other measures to quantify the quality of the reconstruction. Indeed, from Figure 6, one may observe that the overall behavior of the transversal displacement is captured even with only 5 POMs, the effect of bottom-hole impact being the main source of error. Another measure of the reconstruction quality was then considered, consisting of the time average of the relative error modulus between the reconstructed response v_R and the response of the full model v_F, $e = \sum_{j=1}^{M} |1 - v_F^j / v_R^j| / M$. Using this measure, one may see that using only the first 5 POMs leads to a reconstruction within 14% response error. This error drops to 8%, 3% and less than 1% when using the first 9, 15 and 30 POMs respectively. The zoomed window in Figure 6 shows that there is a clear improvement in the reconstruction of the response when the number of POMs is increased. In fact, when using the first 30 POMs one may capture precisely all the micro-impacts observed in the response. Nevertheless, although using only the first 15 POMs leads to small differences in the response inside the impact region, one may observe that the main micro-impacts effects are accounted for since this reconstructed response follows almost exactly the full model response just after the impact. This means that this reconstruction, within a 3% error, may be reasonably accurate to consider only the first 15 POMs in the reduced order model.

4. CONCLUSIONS

The oscillations of a non-rotating drillstring, represented here by a vertical slender beam, clamped in its upper extreme, pinned in its lower one and constrained inside an outer cylinder in its lower portion, were studied. The beam was supposed as being subjected to distributed axial loads, due to its own weight, leading to geometric softening of its lower portion and, thus, to a large number of vibroimpacts with the outer cylinder. It was shown that one should account for the axial displacement dynamics, using non-linear strain-displacement relations, since the axial/bending dynamical coupling is very important in slender beams dynamics. In particular, the micro-impacts, accompanying the bottom-hole impacts and mainly due to the beam compressive softening, were well represented only by the non-linear model. Moreover, standard linear beam models yield false predictions of the reaction forces at the drillstring bottom position, that is the forces at the formation.

Then, the KL expansion was applied to the simulated dynamics to obtain additional information on the system through analysis of the POMs and POVs and also to construct an optimal reduced order model. The results have shown that at least 15 POMs are required to reconstruct the dynamics of the impacting drillstring under a 3% error margin. This result is encouraging if one compares the dimension of the reduction basis (15) with that of the original FE model (87). Future works are being directed to the application of the reduced order model to other external and loading conditions.

5. ACKNOWLEDGMENTS

The authors gratefully acknowledge the financial support of "Fundação Carlos Chagas Filho de Amparo à Pesquisa do Estado do Rio de Janeiro" (FAPERJ), through grants nos. 172.038/00, 151.188/00 and 150.687/00.

6. REFERENCES

Azeez, M.F.A. and Vakakis, A.F., 2001, "Proper orthogonal decomposition (POD) of a class of vibroimpact oscillations", Journal of Sound and Vibration, Vol. 240, No. 5, pp. 859–889.

Kane, T.R., Ryan, R.R., and Banerjee, A.K., 1987, "Dynamics of a cantilever beam attached to a moving base", Journal of Guidance, Control, and Dynamics, Vol. 10, No. 2, pp. 139–151.

Sharf, I., 1995, "Geometric stiffening in multibody dynamics formulations", Journal of Guidance, Control, and Dynamics, Vol. 18, No. 4, pp. 882–890.

Simo, J. and Vu-Quoc, L., 1987, "The role of non-linear theories in transient dynamic analysis of flexible structures", Journal of Sound and Vibration, Vol. 119, No. 3, pp. 487–508.

Sirovich, L., 1987, "Turbulence and the dynamics of coherent structures part I: coherent structures", Quarterly of Applied Mathematics, Vol. 45, No. 3, pp. 561–571.

Sotomayor, G.P.G., Plácido, J.C., and Cunha, J.C., 1997, "Drill string vibration: How to identify and suppress", In Proceedings of 5^{th} Latin American and Caribbean Petroleum Engineering Conference and Exhibition, paper no. SPE 39002.

Steindl, A. and Troger, H., 2001, "Methods for dimension reduction and their application in non-linear dynamics", International Journal of Solids and Structures, Vol. 38, No. 10-13, pp. 2131–2147.

Trindade, M.A. and Sampaio, R., 2002, "Dynamics of beams undergoing large rotations accounting for arbitrary axial deformation", to appear in the Journal of Guidance, Control, and Dynamics.

Wolter, C. and Sampaio, R., 2001, "Bases de Karhunen-Loève: Aplicações à mecânica dos sólidos", In Proceedings of the 1^{st} Brazilian Workshop in Aplications of Dynamics and Control (Aplicon 2001), ABCM/SBMAC, São Carlos, pp. 129–172.

Wolter, C., Trindade, M.A., and Sampaio, R., 2001, "Obtaining mode shapes through the Karhunen-Loève expansion for distributed-parameter linear systems", In Proceedings of the 16^{th} Brazilian Congress of Mechanical Engineering, ABCM, Uberlândia, Vol. 10, pp. 444–452.